Valley filtering in graphene with a Dirac gap

Feng Zhai
Center of Statistical and Theoretical Condensed Matter Physics and Department of Physics, Zhejiang Normal University, Jinhua 321004, China

Kai Chang
SKLSM, Institute of Semiconductors, Chinese Academy of Sciences, P.O. Box 912, 100083, Beijing, China

(Received 10 November 2011; revised manuscript received 27 March 2012; published 9 April 2012)

We explore valley filtering in a two-terminal graphene system with a Dirac gap. For such a system with a constant Dirac gap, it is found that the presence of a valley-polarized output current requires both a magnetic barrier and an electric potential. For the magnetic-electric barrier generated by a single ferromagnetic stripe, a remarkable valley polarization can be achieved and is tunable by gate voltages. The generated valley polarization can be detected from the Hall measurement in the outgoing region [Phys. Rev. Lett. **99**, 236809 (2007)].

DOI: 10.1103/PhysRevB.85.155415 PACS number(s): 72.80.Vp, 73.43.Cd, 75.70.Ak, 85.35.−p

I. INTRODUCTION

Since its discovery,[1] graphene, a two-dimensional honeycomb lattice made of carbon atoms, has attracted a great interest[2,3] as a promising candidate material for the post-silicon nanoelectronics. Most fascinating electronic properties of graphene arise from its Dirac-like, massless excitations around the K and K' valleys of the Brillouin zone. Klein tunneling is a typical consequence of this peculiar band structure. It allows carriers to transmit any electrostatic barrier at normal incidence and thus may limit the performance of graphene-based conventional electronic devices like diodes and transistors. A natural approach to suppress Klein tunneling is to open a Dirac gap, i.e, a bulk gap near the Dirac points. The Dirac gap has been created by means of the sublattice-dependent graphene-substrate interaction.[4–9] Its size depends on the experimental details and ranges from a few to hundreds of meV. A spatially-varying Dirac gap has been reported in Ref. 6, which may be utilized to form a graphene quantum dot[10] without the application of external electric and magnetic fields.

The twofold valley degeneracy in graphene's band structure suggests another routine of carbon-based electronics, dubbed valleytronics.[11–18] The independent valley states are related by the time-reversal symmetry. Due to the large momentum separation of two valleys, valley information is immune to the disturbance of slowly varying potentials and magnetic fields. It could be preserved over a long distance.[19] A prerequisite for valleytronic applications is to create and detect valley-polarized currents. The seminal proposal of valley filters[11] relies on perfect zigzag nanoribbons, which would harden its experimental realization. Several valley filtering schemes based on bulk graphene have been put forward, utilizing valley-dependent trigonal warping of the carrier dispersion,[13,14] strain-induced pseudomagnetic fields,[15–17] and line defects.[18] For these proposed devices, the detection of the generated valley polarization requires additional elaborate setup.

In this work, we investigate valley-resolved transport properties of a graphene membrane with a Dirac gap. We find that under the modulation of proper magnetic-electric barriers, electrons from K and K' valley exhibit distinct transmission features, resulting in a remarkable valley polarization of output current. It has been shown theoretically that in graphene with broken inversion symmetry, the injection of valley-polarized current will generate a transverse voltage,[20] in a similar way as inverse spin-Hall effect.[21] Therefore, the valley polarization produced by our proposed device can be detected directly from the Hall measurement in the outgoing region [see Fig. 1(a)].

II. MODEL AND FORMALISM

We consider a graphene membrane in the (x, y) plane covered by a thin dielectric layer, as illustrated in Fig. 1(a). By means of substrate engineering, a Dirac gap 2Δ is created and may be position dependent,[4–9] i.e., $\Delta = \Delta(\mathbf{r})$. The Dirac electrons therein are subject to the modulations of a local perpendicular magnetic field $\mathbf{B}$ and electrostatic potential U. The magnetic field is assumed to vary only along the x axis, which can be generated by depositing ferromagnetic metal (FM) or superconducting (S) materials on top of the dielectric layer, as is the way in semiconductor heterostructures.[22,23] The magnetic vector potential will be taken in the Landau gauge, $\mathbf{A} = A_y(x)\mathbf{e}_y$ with $dA_y/dx = B_z(x)$. The scalar potential $U = U(x)$ is induced by the FM or S gate(s) and perhaps additional normal metal gates. In the incident and outgoing regions ($\alpha = i,o$), all potentials are uniform: $\Delta = \Delta_\alpha$, $U = U_\alpha$, and $A_y = A_{y\alpha}$.

The low-energy effective Hamiltonian reads[2]

$$H = \sum_\tau \int d\mathbf{r}\Psi_\tau^+[v_F\sigma\cdot(\mathbf{p}+e\mathbf{A}) + \tau\Delta\sigma_z + U\sigma_0]\Psi_\tau, \quad (1)$$

where $\tau = \pm 1$ labels the K and K' valleys, the valley-resolved spinor $\Psi_+ = (\Psi_A, \Psi_B)^T$ and $\Psi_- = (-\Psi'_B, \Psi'_A)^T$ contain electron fields in two carbon sublattices A and B, v_F is the Fermi velocity, $\sigma = (\sigma_x, \sigma_y)$ together with σ_z are Pauli matrices, σ_0 is a unit matrix, and $\mathbf{p} = -i\hbar(\partial_x, \partial_y)$ is the in-plane momentum of electrons. For convenience, hereafter all quantities will be expressed in dimensionless units by means of the length scale $l_B = [\hbar/(eB_0)]^{1/2}$ and energy scale $E_0 = \hbar v_F/l_B$. For a typical magnetic field $B_0 = 0.1$ T, the reduced units are $l_B = 81.1$ nm and $E_0 = 7.0$ meV.

The translational invariance along the y direction enables us to write the wave functions as $\Psi_\tau(\mathbf{r}) = \exp(ik_y y)\psi_\tau(x)$,

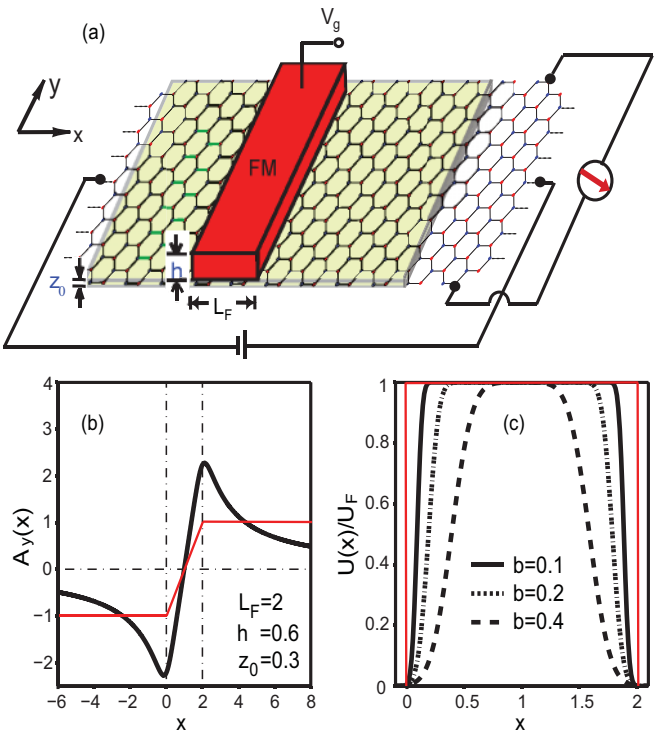

FIG. 1. (Color online) (a) Schematic of the proposed graphene valley filter. The motion of electrons therein is modulated by both the substrate-induced sublattice potential and the magnetic-electric barrier provided by a single FM gate. The generated valley polarization can be detected by the inverse valley-Hall effect. (b) and (c) Profiles of the magnetic vector potential and scalar potential, which are generated by the FM gate (black thick lines) or for a simplified square magnetic-electric barrier (thin solid lines in red).

where k_y is the conserved transverse wave vector, and $\psi_\tau = (\psi_{\tau+},\psi_{\tau-})^T$ obeys $H_\tau(k_y)\psi_\tau = E\psi_\tau$ with

$$H_\tau(k_y) = -i\partial_x\sigma_x + (k_y + A_y)\sigma_y + \tau\Delta\sigma_z + U\sigma_0. \quad (2)$$

For an electron in τ valley with energy E and transverse wave vector k_y, we denote the transmission probability as $T_\tau(E,k_y)$. The scattering matrix method[24] is adopted to calculate T_τ. For a given Fermi energy E_F, the valley-related zero-temperature conductance is calculated from

$$G_\tau = G_0\int_{k_{y-}}^{k_{y+}} T_\tau(E_F,k_y)dk_y, \quad (3)$$

where $G_0 = e^2L_y/(\pi h)$ is the conductance unit with L_y the dimensionless sample size along the y direction, and $k_{y\pm} = \pm\sqrt{(E_F - U_i)^2 - \Delta_i^2} - A_{yi}$. Once G_τ is obtained, it is straightforward to calculate the total conductance $G = G_+ + G_-$ and valley polarization $P = (G_+ - G_-)/G$.

III. NECESSARY CONDITIONS FOR VALLEY FILTERING

We begin with the symmetry analysis[25] on the Hamiltonian (2). When the magnetic barrier is absent or replaced by the strain-induced pseudomagnetic field,[3] this Hamiltonian satisfies

$$\sigma_x H_\tau(k_y)\sigma_x^{-1} = H_{-\tau}(-k_y), \quad (4)$$

which indicates $T_\tau(E,k_y) = T_{-\tau}(E,-k_y)$. This together with Eq. (3) results in a vanishing valley polarization P. Thus the presence of a magnetic barrier is necessary to obtain a valley-polarized current from the considered system.

For a constant Dirac gap, a finite valley polarization requires not only magnetic barriers but also electric barriers. This can be readily seen from the equation that the two components of the spinor ψ_τ satisfy:

$$\left[\partial_x^2 + F_0^\pm + F_\tau^\pm(\pm k_y \pm A_y - \partial_x)\right]\psi_{\tau\pm} = 0. \quad (5)$$

Here

$$F_\tau^\pm = (E - U \pm \tau\Delta)^{-1}(\pm\tau\partial_x\Delta - \partial_x U), \quad (6)$$

$$F_0^\pm = (E-U)^2 - \Delta^2 - (k_y + A_y)^2 \mp \partial_x A_y. \quad (7)$$

In the case that $\partial_x\Delta = 0$ and $\partial_x U = 0$, F_τ vanishes and then no valley polarization can be created.

For the potential profiles with certain experimentally realizable symmetries, the valley polarization may also disappear. We consider two typical situations in which the vector potential can be chosen to be either symmetric or antisymmetric with respect to a central line $x = x_c$, i.e., $R_x A_y = \pm A_y$, while the Dirac gap and the electric potential have a symmetrical distribution ($R_x\Delta = \Delta$ and $R_x U = U$). Here R_x is the reflection operation $x \to 2x_c - x$. For the case that the vector potential is symmetric, it can be checked that

$$(\sigma_y R_x)H_\tau(k_y)(\sigma_y R_x)^{-1} = H_{-\tau}(k_y). \quad (8)$$

This observation leads to $T_\tau(E,k_y) = T_{-\tau}(E,k_y)$ and then $P = 0$. For the case of an antisymmetric A_y, the operation $\sigma_z R_x$ transforms $H_\tau(k_y)$ into $H_\tau(-k_y)$, which implies $T_\tau(E,k_y) = T_\tau(E,-k_y)$. We will show that P can be finite in this case.

IV. NUMERICAL RESULTS AND DISCUSSIONS

Firstly, we derive an analytical solution of Eq. (2) for a square magnetic-electric barrier[26,27] within the stripe $0 < x < L$, i.e.,

$$\mathbf{B}(\mathbf{r}) = B_s\Theta(x)\Theta(L-x), \quad (9)$$

$$U(\mathbf{r}) = U_s\Theta(x)\Theta(L-x). \quad (10)$$

Here $\Theta(x)$ is the Heaviside step function, and $B_s \neq 0$ and U_s are constant. The value of the Dirac gap in the barrier region and the lead region is denoted as $2\Delta_b$ and 2Δ, respectively. The longitudinal wave vector of the incident/outgoing wave reads $k_{xi/o} = \mathrm{sgn}(E + \tau\Delta)\sqrt{E^2 - \Delta^2 - k_{yi/o}^2}$ with $k_{yi/o} = k_y \mp B_s L/2$. It is useful to introduce the notations

$$\gamma_\tau = \sqrt{2B_s}(E + \tau\Delta)/(E + \tau\Delta_b - U_s), \quad (11)$$

$$\nu = \left[(E-U_s)^2 - \Delta_b^2\right]/(2B_s), \quad (12)$$

$$u_p^{l\pm} = D_p(\pm k_y\sqrt{2/B_s}), \quad (13)$$

$$u_p^{r\pm} = D_p[\pm\sqrt{2B_s}(L + k_y/B_s)], \quad (14)$$

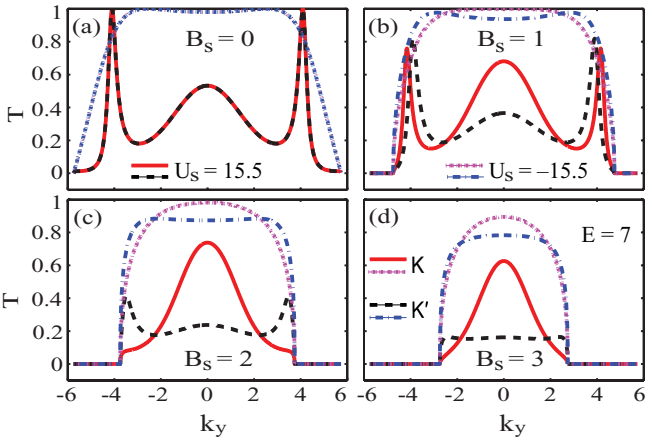

FIG. 2. (Color online) T_+ and T_- as a function of the transverse wave vector for electrons traversing a square magnetic-electric barrier under $U_S = \pm 15.5$ and $B_S = 0$, 1, 2, and 3. The incident energy is fixed at $E = 7$. The barrier width is $L = 2$.

where $D_p(x)$ is the parabolic cylinder function of order p. The transmission probability T_τ is given by

$$T_\tau = \frac{4k_{xi}k_{xo}\left(u^{r+}_{\nu-1}u^{r-}_{\nu} + u^{r-}_{\nu-1}u^{r+}_{\nu}\right)^2}{\left|k_i^- A^{\nu}_{\nu-1} + k_o^+ A^{\nu-1}_{\nu} - i\gamma_\tau A^{\nu}_{\nu} + \frac{i}{\gamma_\tau}k_i^- k_o^+ A^{\nu-1}_{\nu-1}\right|^2}, \quad (15)$$

where $A^q_p = u^{l-}_p u^{r+}_q - (-1)^{p-q}u^{l+}_p u^{r-}_q$, $k_i^- = k_{xi} - ik_{yi}$, and $k_o^+ = k_{xo} + ik_{yo}$. The valley dependence of the transmission in Eq. (15) comes only from the parameter γ_τ defined in Eq. (11). Obviously, $T_+ = T_-$ when both $U_s = 0$ and $\Delta_b = \Delta$ are met, in agreement with our previous analysis. Note that $\gamma_+ \neq \gamma_-$ in the case of $U(\mathbf{r}) = 0$, but $\Delta_b \neq \Delta$. This observation indicates that a combination of a position-dependent Dirac gap and a local magnetic field can generate a finite valley polarization without the need of an electric barrier [see also Eq. (6)]. Details on this respect will be reported elsewhere.

Without specification, we take a constant Dirac gap with a moderate size $2\Delta = 8$.[4–9] For electrons with a typical energy $E = 7$ traversing the square magnetic-electric barrier, the transmission probability is plotted in Fig. 2 as a function of k_y. The transmission shows a mirror symmetry about $k_y = 0$ and becomes valley independent at $B_s = 0$ [see Fig. 2(a)], as required by the symmetry of the considered structure. For the interband tunneling ($U_s > 2\Delta$), remarkable Fabry-Pérot resonances appear due to interference of the counterpropagating channels in the barrier region. For a small $B_s \neq 0$ [Fig. 2(b)], the valley degeneracy of the transmission is lifted ($\gamma_+ \neq \gamma_-$). Thus one can observe a valley splitting of the resonances and a valley-dependent resonant enhancement and suppression. With the increase of the magnetic barrier height [Figs. 2(b)–2(d)], some resonant peaks move toward the large $|k_y|$ region and disappear eventually, while the difference between T_+ and T_- can be enlarged. The interband tunneling leads to a more remarkable valley contrast of the transmission than the intraband tunneling ($U_s < 0$). This can be understood from the dependence of $\gamma_\pm$ on the height of the magnetic barrier and electric barrier. Since the conductance G_τ in Eq. (3) is proportional to the integral of T_τ over k_y, the valley dependence of the transmission shown in Figs. 2(b)–2(d) indicates a finite valley polarization.

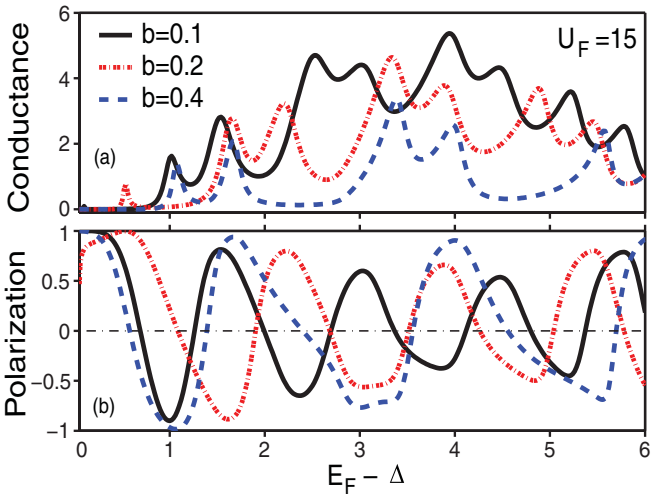

FIG. 3. (Color online) (a) Conductance and (b) valley polarization as a function of the Fermi energy for the system depicted in Fig. 1(a). $U_F = 15$.

The rectangular magnetic barrier may be viewed as a simplified magnetic field profile formed by means of the superconducting Meisser effect.[23,26] In realistic cases, the magnetic barrier and electric potential should vary smoothly on the scale of the graphene lattice constant. For definiteness, we turn our attention to the magnetic-electric barrier generated by a single FM gate. The latter has a rectangular cross section [see Fig. 1(a)] and a magnetization $\mathbf{M}$ along the z axis.[22] Its width, height, magnetization strength, and distance to the graphene plane are fixed respectively at $L_F = 2$, $h = 0.6$, $\mu_0 M = 1.8$ T (for cobalt material), and $z_0 = 0.3$. The electric potential induced by the FM gate is modeled as $U_F a(x)$, where

$$a(x) = \{\mathrm{erf}(2x/b - 2) + \mathrm{erf}[2(L_F - x)/b - 2]\}/2, \quad (16)$$

$\mathrm{erf}(x)$ is the error function, the parameter b ($0 < b < L_F/4$) determines the width of the crossover region, and U_F is the amplitude. The smooth profiles of the vector potential[26] and scalar potential generated by the FM gate are shown in Figs. 1(b) and 1(c).

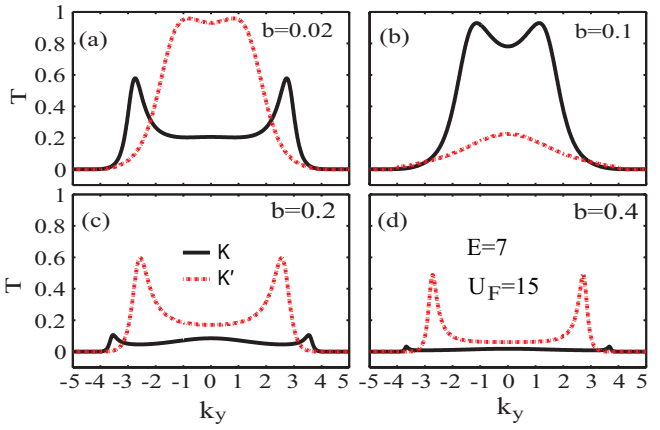

FIG. 4. (Color online) T_+ and T_- as a function of the transverse wave vector for electrons traversing the system depicted in Fig. 1(a) with parameter $b = 0.02$, 0.1, 0.2, and 0.4. $E = 7$ and $U_F = 15$.

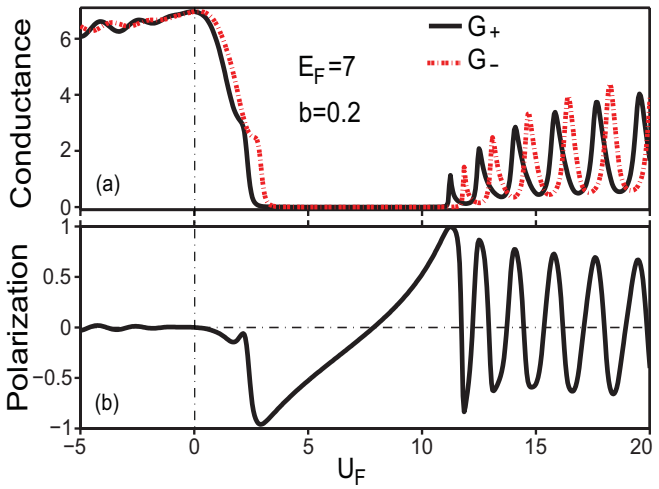

FIG. 5. (Color online) (a) Valley-dependent conductance and (b) valley polarization as a function of the height of the electric barrier for the system depicted in Fig. 1(a). $E_F = 7$.

As shown in Fig. 3, the magnetic-electric barrier generated by the FM gate alone is sufficient to obtain a remarkable valley polarization P under a finite conductance. In this figure, a large value of $U_F = 15 > 2\Delta$ is taken so that the interband tunneling happens. The oscillation of the conductance with the Fermi energy E_F comes from the valley-dependent resonant tunneling. Since the adjacent conductance peaks are contributed dominantly by different valleys, the polarity of P alternates with E_F. Note that although our calculations are made at zero temperature, the valley polarization considered here should survive at a finite temperature $T_K < 0.1E_0/k_B \sim 8$ K. It can be seen that the parameter b of the electric barrier has a drastic effect on both the conductance and the valley polarization. With the increase of b, in general the conductance is lowered while the valley polarization is enhanced. This indicates that a smooth electric potential would be more helpful for valley filtering.

These features can be understood as follows. For a given incident energy E and all k_y values, there is no propagating mode in the classically forbidden region $[x_-,x_+]$ and $[L_F - x_+, L_F - x_-]$. Here $x_\pm \in [0,2b]$ satisfies $a(x_\pm) = (E \pm \Delta)/U_F$. As b increases, the width of such two barrierlike regions becomes larger and larger. Accordingly, the conductance decreases. On the other hand, the valley polarization is determined by the valley-dependent effective potential F_τ [Eq. (6)], which exists in a wider region for a larger b. Thus the increase of b can enhance the valley polarization. The variation of the conductance peaks with b can be explained in a similar way. To get a better feeling on the b dependence of the resonant tunneling, we plot in Fig. 4 the valley-dependent transmission for a typical incident energy $E = 7$ and several b values.

The valley polarization is also tunable by gate voltages, as shown in Fig. 5. For $U_F < E_F - \Delta$ (intraband tunneling), the valley polarization is remarkable only when the wave-vector filtering of the magnetic barrier[26,27] plays a major role in the transport process. For $U_F > E_F + \Delta$, one can observe a series of valley-splitting conductance peaks with large peak-valley ratios. The distance between the nearest G_+ peak and G_- peak is determined by the magnetic barrier. Note that the two classically forbidden regions become thinner as U_F increases from $E_F + \Delta$. Thus the valley polarization shows a decaying oscillation with U_F.

Finally, we give some remarks. In Ref. 28 the bound states of a circular quantum dot based on gapped graphene has been studied, which shows a valley splitting under a homogeneous perpendicular magnetic field. In our model with an electric potential well, valley-dependent bound states may appear as well for electrons in the conduction band. However, they are always below the incident energy of electrons from the conduction band. Accordingly, the valley contrast is low, as shown in Figs. 2 and 5. To make those valley-splitting bound states active for valley filtering, we may design more complicated structures such as a combination of an electrostatic double barrier and a magnetic barrier in gapped graphene. In the case of interband tunneling, the valley-selective transmission resonances (in Figs. 2–5) are related to the valley-splitting quasibound states of electrons in the valence band. In realistic graphene ribbons, edge orientation and roughness together with short range disorder will result in valley mixing and then a decrease in the degree of valley polarization. The discussion on this unwanted effect is beyond the scope of our model. We believe that the valley polarization shown in the present work should be not degraded substantially under the following two sample conditions: (1) the ribbon width L_y is large enough so that the dominant transport is through the bulk states; (2) the sample size is within the intervalley mean-free path.

V. CONCLUSIONS

We have demonstrated theoretically the valley filtering effect in a two-terminal graphene system with a Dirac gap. The necessary condition to construct such a valley filter is given. We find that a bulk graphene system with a constant Dirac gap, when modulated by a single ferromagnetic stripe on top, can output a remarkable valley polarization. The generated valley polarization is tunable by gate voltages, and can be detected directly from the Hall measurement in the outgoing region. Our findings may shed some light on the realization of graphene valleytronics.

ACKNOWLEDGMENTS

This work was supported by the NSFC Grants No. 11174252, No. 60525405, and No. 10874175.

[1] K. S. Novoselov, A. K. Geim, D. Jiang, Y. Zhang, S. V. Dubons, I. V. Grogorieva, and A. A. Firsov, Science **306**, 666 (2004).

[2] C. W. J. Beenakker, Rev. Mod. Phys. **80**, 1337 (2008).

[3] A. H. Castro Neto, F. Guinea, N. M. R. Peres, K. S. Novoselov, and A. K. Geim, Rev. Mod. Phys. **81**, 109 (2009).

[4]S. Y. Zhou, G.-H. Gweon, A. V. Fedorov, P. N. First, W. A. de Heer, D.-H. Lee, F. Guinea, A. H. Castro Neto, and A. Lanzara, Nat. Mater. **6**, 770 (2007).
[5]S. Kim, J. Ihm, H. J. Choi, and Y. W. Son, Phys. Rev. Lett. **100**, 176802 (2008).
[6]L. Vitali, C. Riedl, R. Ohmann, I. Brihuega, U. Starke, and K. Kern, Surf. Sci. **602**, L127 (2008).
[7]G. H. Li, A. Luican, and E. Y. Andrei, Phys. Rev. Lett. **102**, 176804 (2009).
[8]C. Enderlein, Y. S. Kim, A. Bostwick, E. Rotenberg, and K. Horn, New. J. Phys. **12**, 033014 (2010).
[9]N. T. Cuong, M. Otani, and S. Okada, Phys. Rev. Lett. **106**, 106801 (2011).
[10]G. Giavaras and F. Nori, Appl. Phys. Lett. **97**, 243106 (2010); Phys. Rev. B **83**, 165427 (2011); M. Ramezani Masir, A. Matulis, and F. M. Peeters, *ibid*. **84**, 245413 (2011).
[11]A. Rycerz, J. Tworzydło, and C. W. J. Beenakker, Nat. Phys. **3**, 172 (2007).
[12]Z. Z. Zhang, K. Chang, and K. S. Chan, Appl. Phys. Lett. **93**, 062106 (2008).
[13]J. L. Garcia-Pomar, A. Cortijo, and M. Nieto-Vesperinas, Phys. Rev. Lett. **100**, 236801 (2008).
[14]J. M. Pereira Jr., F. M. Peeters, R. N. Costa Filho, and G. A. Farias, J. Phys.: Condens. Matter **21**, 045301 (2009).
[15]F. Zhai, X. F. Zhao, K. Chang, and H. Q. Xu, Phys. Rev. B **82**, 115442 (2010); F. Zhai, Y. L. Ma, and Y.-T. Zhang, J. Phys.: Condens. Matter **23**, 385302 (2011).
[16]A. Chaves, L. Covaci, Kh. Yu. Rakhimov, G. A. Farias, and F. M. Peeters, Phys. Rev. B **82**, 205430 (2010).
[17]Z. H. Wu, F. Zhai, F. M. Peeters, H. Q. Xu, and K. Chang, Phys. Rev. Lett. **106**, 176802 (2011); F. Zhai, Y. L. Ma, and K. Chang, New J. Phys. **13**, 083029 (2011).
[18]D. Gunlycke and C. T. White, Phys. Rev. Lett. **106**, 136806 (2011).
[19]The intervalley mean-free path is estimated to be of the order 1 μm, see, e.g., F. V. Tikhonenko, D. W. Horsell, R. V. Gorbachev, and A. K. Savchenko, Phys. Rev. Lett. **100**, 056802 (2008).
[20]D. Xiao, W. Yao, and Q. Niu, Phys. Rev. Lett. **99**, 236809 (2007).
[21]E. Saitoh, M. Ueda, H. Miyajima, and G. Tatara, Appl. Phys. Lett. **88**, 182509 (2006); S. O. Valenzuela and M. Tinkham, Nature (London) **442**, 176 (2006).
[22]See, for examples, A. Nogaret, S. J. Bending, and M. Henini, Phys. Rev. Lett. **84**, 2231 (2000); A. Nogaret, D. N. Lawton, D. K. Maude, J. C. Portal, and M. Henini, Phys. Rev. B **67**, 165317 (2003); J. Hong, S. Joo, T.-S. Kim, K. Rhie, K. H. Kim, S. U. Kim, B. C. Lee, and K.-H. Shinc, Appl. Phys. Lett. **90**, 023510 (2007); A. Tarasov, S. Hugger, H. Y. Xu, M. Cerchez, T. Heinzel, I. V. Zozoulenko, U. Gasser-Szerer, D. Reuter, and A. D. Wieck, Phys. Rev. Lett. **104**, 186801 (2010).
[23]For a review, see S. J. Lee, S. Souma, G. Ihm, and K. J. Chang, Phys. Rep. **394**, 1 (2004).
[24]H. Xu, Phys. Rev. B **50**, 8469 (1994).
[25]F. Zhai and H. Q. Xu, Phys. Rev. Lett. **94**, 246601 (2005).
[26]A. Matulis, F. M. Peeters, and P. Vasilopoulos, Phys. Rev. Lett. **72**, 1518 (1994).
[27]A. DeMartino, L. Dell'Anna, and R. Egger, Phys. Rev. Lett. **98**, 066802 (2007).
[28]P. Recher, J. Nilsson, G. Burkard, and B. Trauzettel, Phys. Rev. B **79**, 085407 (2009).